



Research Article

Experimental Study on the Anisotropy of Layered Rock Mass under Triaxial Conditions

Long Cheng ¹, Hui Wang ¹, Xu Chang,² Yewei Chen,³ Feilu Xu,⁴
Bafang Zhang,⁵ and Jiawei An³

¹School of Civil Engineering, Henan Polytechnic University, Jiaozuo 454000, China

²School of Civil Engineering, Huaqiao University, Xiamen 361021, China

³China Construction Fourth Engineering Division Co., Ltd., Guangzhou 510000, China

⁴Xiamen Luhengda Construction Engineering Co., Ltd., Xiamen 361021, China

⁵Jianyan Test Group Co., Ltd., Xiamen 361021, China

Correspondence should be addressed to Hui Wang; wwhui@hpu.edu.cn

Received 15 August 2021; Accepted 29 November 2021; Published 15 December 2021

Academic Editor: Han-Cheng Dan

Copyright © 2021 Long Cheng et al. This is an open access article distributed under the Creative Commons Attribution License, which permits unrestricted use, distribution, and reproduction in any medium, provided the original work is properly cited.

Weak and hard inhomogeneous rock formations are typically encountered during tunnel excavations. The physical and mechanical properties and geological conditions of these rock formations vary significantly; thus, it is crucial to investigate the mechanical characteristics of deep bedded composite rock formations. Three-dimensional (3D) scanning and 3D printing were used to prepare composite rock specimens to simulate natural rock laminae. Triaxial compression tests were conducted to determine the influence of the bedding angle, rock composition, and confining pressure on the mechanical properties of the composite rock specimens. The anisotropic strength characteristics and the damage patterns of the composite rock specimens were analyzed under different confining pressures, and the failure mechanism during triaxial loading was revealed. The results show that the damage of the composite rock specimens with a bedding structure depends on the bedding dip angle and the rock formation. The stress-strain curves and peak strengths of the composite rock specimens have anisotropic characteristics corresponding to their failure modes. As the bedding dip angle increases, the peak strength of the three groups of specimens first decreases and then increases under different confining pressure levels. The compressive strength has a nonlinear relationship with the confining pressure, and the difference between the compressive strengths of specimens with different inclination angles decreases as the confining pressure increases. The Hoek–Brown strength criterion is a good predictor of the nonlinear increase in peak strength of the composite rock specimens under different confining pressures. The specimen with a $\beta = 60^\circ$ dip angle shows the most significant increase in the strength difference with increasing confining pressure. The results can be used as a reference for testing and analyzing the anisotropic mechanical properties of bedded rock masses.

1. Introduction

Layered rocks are extensively encountered in mining, civil engineering, and geological engineering projects [1–4]. The rocks' bedding planes are weak links that may result in geological disasters, such as landslides, collapses, and water bursts. Figure 1 shows a weak and hard inhomogeneous stratum encountered during tunneling in a practical project. Therefore, the mechanical performance of layered rocks has become a crucial issue in recent decades. An accurate

determination of the deformation characteristics and failure mechanics requires an in-depth understanding of the influence of the bedding plane orientation and nonuniform deformation of layers on the strength characteristics of composite rock formations.

Numerous studies have been conducted to investigate the mechanical behavior of layered rocks. Tavallali and Vervoort [5] noted that the crack pattern of layered rocks under compression consisted of sliding along the bedding plane and subvertical cracks. Debecker and Vervoort [6]

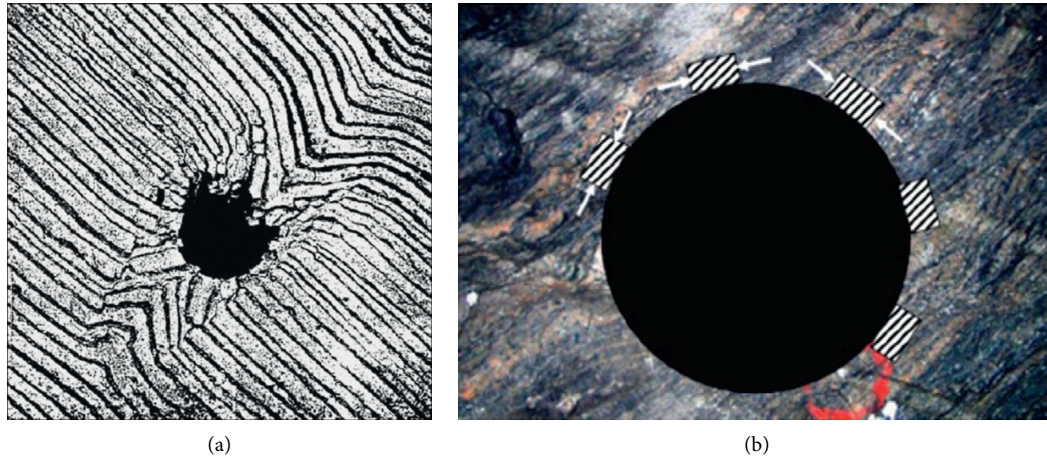


FIGURE 1: Failure mode and stress state of layered rock surrounding a wellbore or tunnel. (a) Wellbore failure in areas of steep, thin circulating zones [1]. (b) Stress states around a tunnel in a layered rock mass [4].

used acoustic emission (AE) data to describe the crack evolution of layered rocks. Many investigations have been conducted to predict strength changes in layered rock as a result of the layer orientation. The weakness in the in-lane directions and the associated theory on variable cohesive strength have been used to describe the influence of weak bedding on the strength of layered rocks [7, 8]. This model was further modified to accommodate changes in the friction angle within the layered rocks [9]. Nova [10] proposed a generalized failure criterion to describe the failure strength of layered rocks in three-dimensional (3D) stress states. It is difficult to obtain adequate layered rock specimens with uniform properties and an ideal layered structure because of the high variability of natural rock arising from the formation processes and geological environments. Tien and Tsao [11] proposed a technique for preparing layered rocks and conducted experiments and analyses to determine the rocks' failure modes and specimen strengths. Chang and Deng [12] investigated the failure mechanisms of unreinforced and reinforced layered rocks with various layer dip angles using AE tests to obtain the failure modes and load-displacement responses.

These studies significantly advanced the understanding of the mechanical behavior of layered rocks. It should be noted that the macro- and microstructure characteristics of the interface between the rock layers were not considered in these studies. Therefore, our understanding of the fracture behavior of rock layers is limited, and the prediction of the mechanical performances of layered rock may be inaccurate. 3D printing (3DP) technology has developed rapidly in recent years and can be used to create structurally complex 3D objects. Several scholars [13–16] have utilized 3DP in their research on rock mechanics. Therefore, this study uses 3D scanning of natural rock laminae, mortar casting, and 3DP to produce rock specimens with bedded rock laminae to study the mechanical response of the composite rock specimens under triaxial loading conditions. The stress-strain curves, deformation, and failure modes of

the composite rock specimens with different bedding dip angles, different rock formations, and different confining pressures are analyzed. The Mohr–Coulomb criterion and the Hoek–Brown criterion are used to fit the test results and analyze the effects of the bedding dip angle and confining pressure on the anisotropic characteristics of the bedded rock mass.

2. Specimen Preparation

The hardness of the rocks in the engineering rock classification standard [17] is used as the basis for sample preparation. The initial strengths of the soft and hard rocks in the composite rock formations were approximately 10 MPa, 20 MPa, and 30 MPa. The physical and mechanical parameters of the soft and hard rocks are listed in Table 1. The combinations are Group AA, Group AB, and Group AC. It should be noted that soft and hard rocks are relative concepts in this paper and are used only to distinguish between materials of different strengths.

The bedding plane of natural rock laminae was obtained by splitting a kilim rock, performing 3D scanning of the layers, and symmetrically combining the layers using 3DP to obtain a natural bedding plane with a dimension of 450 mm × 250 mm × 10 mm. A rectangular plastic mold with internal dimensions of 450 mm × 250 mm × 200 mm was used for preparing the composite specimen. During the pouring process, the mold was placed on a vibrating machine to compact the mix. The printed specimen was pressed onto the mortar to provide the morphological characteristics of a natural bedding plane. After 5 h of drying, the surface was sufficiently imprinted, and the bedding plane was removed before continuing with the next layer. The raw materials used in the tests and the pouring, drying, and processing methods were consistent to ensure uniform bedded composite rock specimens. Black ink was added to the water when the hard rock layers were fabricated to differentiate between soft and hard layers in the same specimen. The process is illustrated in Figure 2.

TABLE 1: The physical and mechanical parameters of the soft and hard rocks.

Material	Density ($\text{g}\cdot\text{cm}^{-3}$)	Ratio (mass ratio) of cement : gypsum : quartz sand : water	Compressive strength (MPa)	Young's modulus (GPa)	Cohesion (MPa)	Friction angle ($^{\circ}$)	Poisson's ratio (%)
Hard rock A	2.07	1 : 0 : 1 : 0.6	34.42	9.87	8.65	33.9	0.19
Soft rock B	1.85	1 : 0.4 : 1 : 0.9	16.50	4.93	5.55	29.6	0.21
Soft rock C	1.64	0.5 : 0.5 : 1 : 0.9	6.91	1.79	2.26	25	0.25

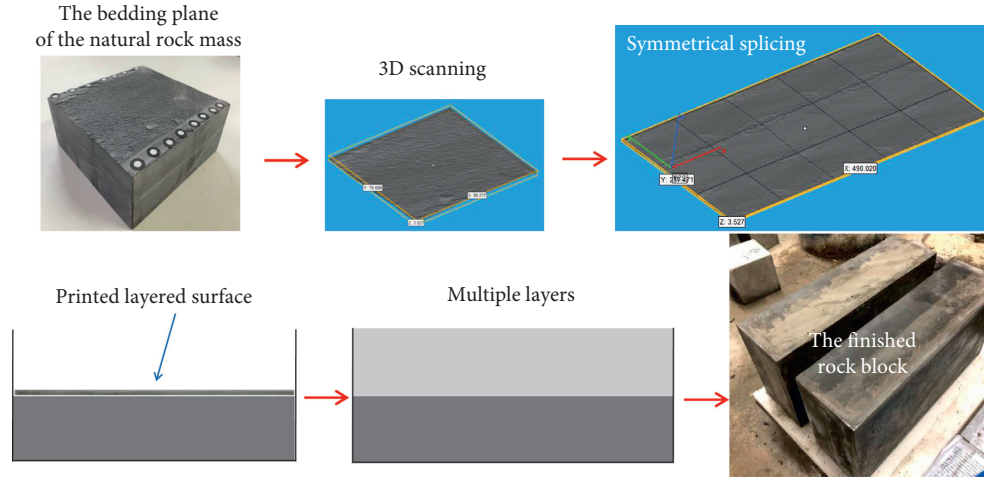


FIGURE 2: The production of the layered rock specimen using 3D scanning and 3D printing.

The finished layered rock specimens were immersed in water for 3 d to reach a certain initial strength. The specimens were drilled at 15 intervals using a 50 mm diameter drill and the drilling method shown in Figure 3; the angle between the loading direction and the normal direction of the laminae is defined as β . The drilled specimens were then fabricated into standard cylindrical specimens of $\Phi 50 \text{ mm} \times L 100 \text{ mm}$ (Φ is diameter of section, L is the length of the specimen), immersed in water, cured to final strength, and subjected to conventional triaxial tests. The completed specimens are shown in Figure 4.

3. Test System and Method

The conventional triaxial compression test was carried out on the RMT-150B testing machine developed by the Institute of Rock and Soil Mechanics, Chinese Academy of Sciences, as shown in Figure 5. A total of four confining pressures (0, 2, 4, and 6 MPa) were used during the test. Seven specimens with different angles were tested under each confining pressure. The confining pressure was loaded in a force-controlled manner, starting with a hydrostatic state ($\sigma_1 = \sigma_2 = \sigma_3$) and loading to a predetermined confining pressure at a loading rate of 2 MPa/min. Subsequently, the confining pressure was kept constant, and the axial force was applied in a displacement-controlled mode at a displacement rate of 0.005 mm/s. The axial force was loaded until the specimens were damaged.

4. Results

4.1. Stress-Strain Curve Analysis. Figure 6 shows the typical stress-strain curves for the group AA specimens ($\beta = 0^{\circ} - 90^{\circ}$) under different confining pressure conditions. It is observed that the specimens undergo an elastic phase, a plastic phase, and a postpeak residual phase during the loading process. Under the effect of the confining pressure, the specimens with the 0° , 15° , 30° , 45° , 75° , and 90° angles exhibit tensile damage with a certain residual strength. After the specimens with the 60° angle reach their peak, the stress rapidly drops, indicating brittle characteristics due to the shear sliding of the specimen along the layered surface during the loading process. This behavior is also observed during the failure.

Figure 7 shows the typical stress-strain curves for the group AB specimens ($\beta = 0^{\circ} - 90^{\circ}$) under different confining pressure conditions. The ductility characteristics of this group of rocks become more pronounced with increasing confining pressure due to the presence of the B-layer soft rock. The specimens with $\beta = 0^{\circ} - 45^{\circ}$ angles only show peaks at low confining pressure (2 MPa), and at high confining pressure (4 MPa, 6 MPa), there is no peak, and the curves show ductility characteristics. The specimens with $\beta = 60^{\circ}$ show peaks at 2 MPa and 4 MPa due to slip damage in the bedding direction and no peaks at 6 MPa.

Figure 8 shows the typical stress-strain curves for Group AC specimens ($\beta = 0^{\circ}$ to 90°) at different confining pressures. There are no peaks in the stress-strain curves for the soft rock at any confining pressures; thus, the strength is the axial

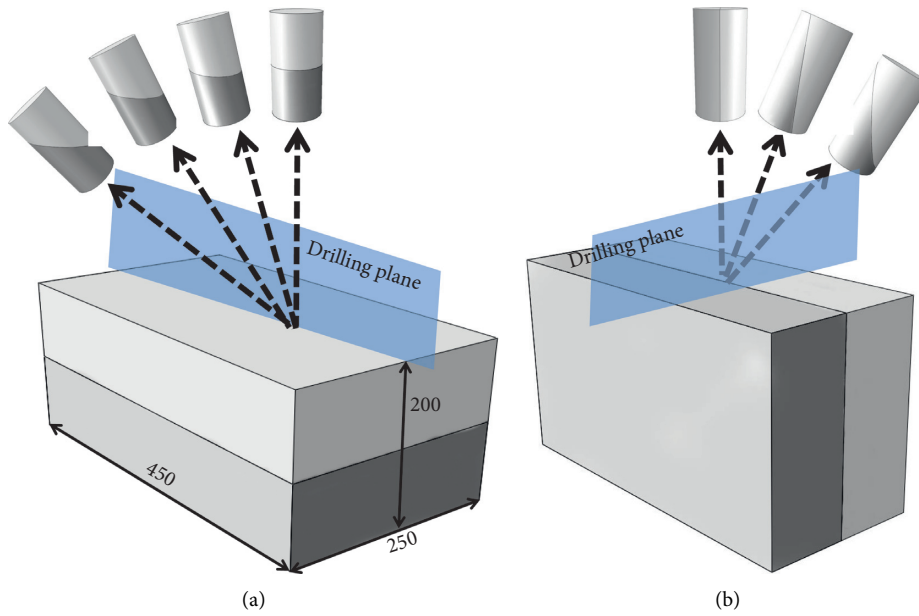


FIGURE 3: Drilling method of the composite rock sample. (a) 0°-45° and (b) 60°-90°.

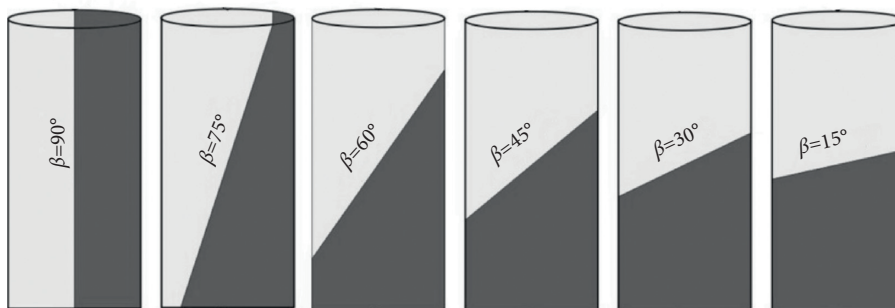
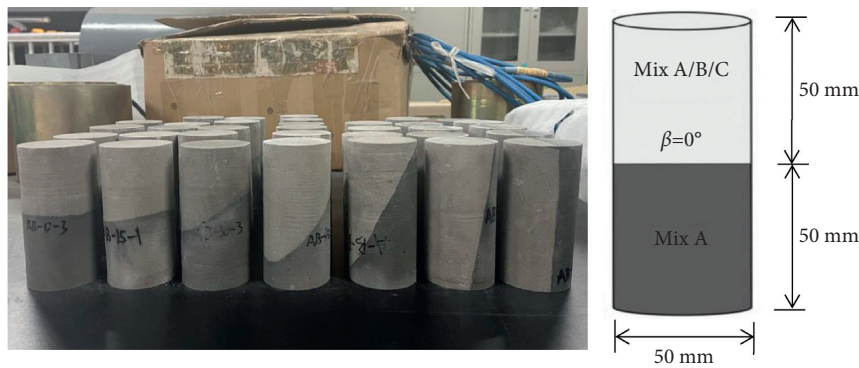


FIGURE 4: The finished layered rock specimens with bedding plane inclination angles β from 0° to 90°.

compressive strength at 0.02% strain. Due to the lower strength of the C-layer soft rock, the specimens ($\beta = 0^\circ$ to 60°) exhibit ductility characteristics at different confining pressures, with no peaks. For the specimens $\beta = 75^\circ$ and 90° , the more brittle hard rock layer A played a supporting role due to the boundary conditions. The soft and hard rock layers deformed almost simultaneously in the axial direction during loading, and shear failure occurred; thus, these two groups of specimens exhibited brittle failure characteristics.

4.2. Effect of Bedding Dip Angle on Strength Characteristics. Figure 9 shows the peak strengths of the three groups of specimens with different dip angles and confining pressures. As the dip angle increases, the peak strengths of the three groups of specimens at different confining pressures show an asymmetric “U” pattern with an initial decrease followed by an increase. In Group AA, the peak strengths of the specimens with $\beta = 0^\circ$ are similar to those with $\beta = 90^\circ$ at each confining pressure, and the peak strength of specimens with



FIGURE 5: The RMT-150B electrohydraulic servo rock test system.

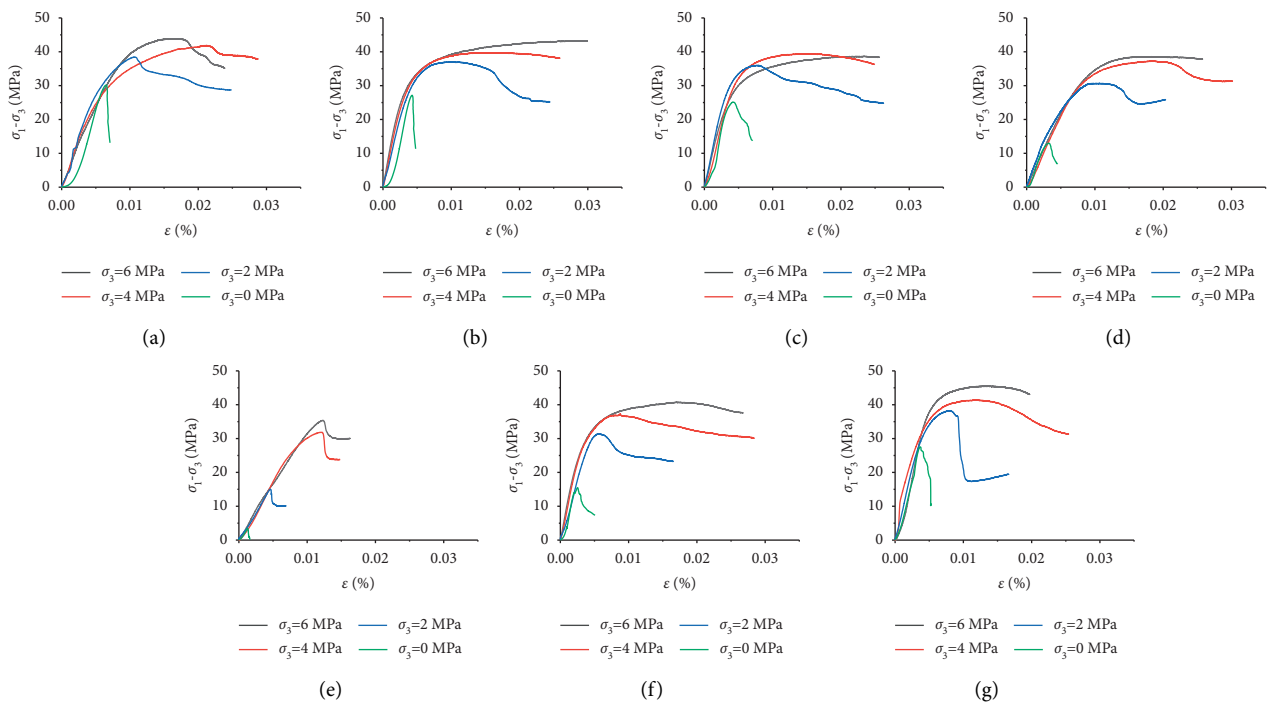


FIGURE 6: Stress-strain curves of Group AA layered composite rock under triaxial compression: (a) $\beta = 0^\circ$, (b) $\beta = 15^\circ$, (c) $\beta = 30^\circ$, (d) $\beta = 45^\circ$, (e) $\beta = 60^\circ$, (f) $\beta = 75^\circ$, and (g) $\beta = 90^\circ$.

a $\beta = 60^\circ$ angle is the lowest, indicating that the strengths of the layered specimens have significant anisotropic characteristics. The patterns are similar for all three groups, but due to the presence of soft rock layers, the peak strengths of the specimens with low dip angles ($\beta = 0^\circ - 60^\circ$) in the two groups are the same under low confining pressure, and there are no anisotropic characteristics. The peak strength of the specimens with large angles ($\beta = 75^\circ - 90^\circ$) is significantly higher than that of the specimens with low angles, especially in the AC group. The reason is that the specimen is fixed at the lower end and pressurized at the upper end in the test, and the boundary conditions of the rock specimens prevent it

from completely sliding along the bedding plane to produce slip damage, which is clearly visible in the damage pattern. The specimens that exhibited splitting as the dominant damage mode had much higher peak stresses than those with complete shear failure and shear failure.

The anisotropy ratio was used to evaluate the degree of anisotropy of the bedded rock mass for the three sets of peak test results [18]. The degree of anisotropy of the laminated rock mass is described by the ratio of $\sigma_{ci(90^\circ)}$, which is the maximum compressive strength at a loading angle of 90° to $\sigma_{ci(\min)}$, that is, the minimum compressive strength at a loading angle between 0° and 90° :

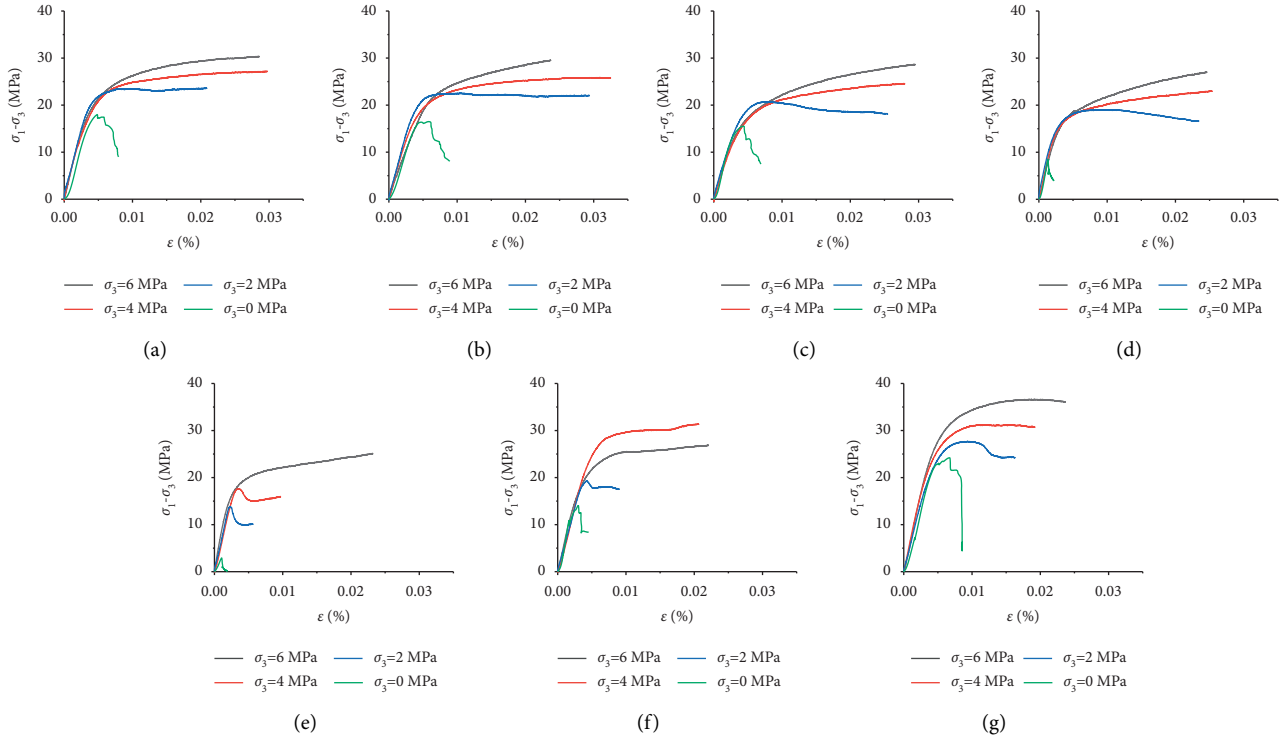


FIGURE 7: Stress-strain curves of Group AB layered composite rock under triaxial compression: (a) $\beta = 0^\circ$, (b) $\beta = 15^\circ$, (c) $\beta = 30^\circ$, (d) $\beta = 45^\circ$, (e) $\beta = 60^\circ$, (f) $\beta = 75^\circ$, and (g) $\beta = 90^\circ$.

$$R_C = \frac{\sigma_{ci(90^\circ)}}{\sigma_{ci(\min)}} \quad (1)$$

The ranges of the anisotropy ratios R_C and the anisotropy classes are listed in Table 2, and the relationship between the anisotropy ratio and the confining pressure is shown in Figure 10. As can be seen from Figure 10, R_C of the specimens in the AA, AB, and AC groups under low confining pressure (2 MPa) are 2.36, 2.2, and 2.02, respectively. All specimens had moderate anisotropy. At high confining pressures (4–6 MPa), R_C for the AA group were 2.21 and 2.1, respectively, whereas R_C for the AB and AC groups decreased to below 2.0 at high confining pressures, falling into the low anisotropy category. The level of anisotropy of all three groups decreased with an increase in the confining pressure. As the confining pressure increased, the specimens containing laminate structures exhibited consolidation, restoring the mechanical continuity of the material; thus, the stratification effect decreased.

4.3. Failure Mode. Figures 11(a)–11(c) show the failure characteristics of the layered composite rocks of Group AA, Group AB, and Group AC, respectively, after the compression tests under different confining pressures. Tien et al. [4] divided the failure modes of composite rock formations under uniaxial loading conditions into two major categories: slip failure in the stratification direction (Type II) and nonslip failure in the stratification direction. In this paper,

the nonslip failure mode is further subdivided into five subcategories, namely, axial splitting (Type I), diagonal shear failure in the bedding plane (Type III), slip and axial splitting along the bedding plane (Type IV), Y-shaped splitting (Type V), and shearing in weak layers (Type VI). The failure modes are shown in Figure 11(d).

The failure modes of the specimens in Group AA with a low dip angle ($\beta = 0^\circ$ – 30°) were similar (Figure 11(a)). At lower confining pressures ($\sigma_3 = 0$ –2 MPa), axial splitting damage occurred (Type I), and the specimens showed longitudinal cracks along the cylindrical surface with significant damage. As the confining pressure increased ($\sigma_3 = 4, 6$ MPa), the failure mode changed to shear failure with an oblique intersection in the bedding plane (Type III). The $\beta = 45^\circ$ specimens subjected to low confining pressure conditions ($\sigma_3 = 0$ –2 MPa) exhibited slip damage along the bedding plane (Type II). When the confining pressure was increased ($\sigma_3 = 4, 6$ MPa), the anisotropy of the specimens weakened with increasing confining pressure, and coupled slip and axial splitting failures occurred along the bedding plane (Type IV). The reason is that the presence of the confining pressure restricted the bedding slip in the stratification direction, and splitting failure occurred in the rock mass. The $\beta = 60^\circ$ – 75° specimens had a larger dip angle, and the failure mode under different confining pressures was slip failure in the stratification direction. For the specimens with $\beta = 75^\circ$, the damage was accompanied by a few splitting cracks along the slip of the bedding plane due to the influence of the boundary

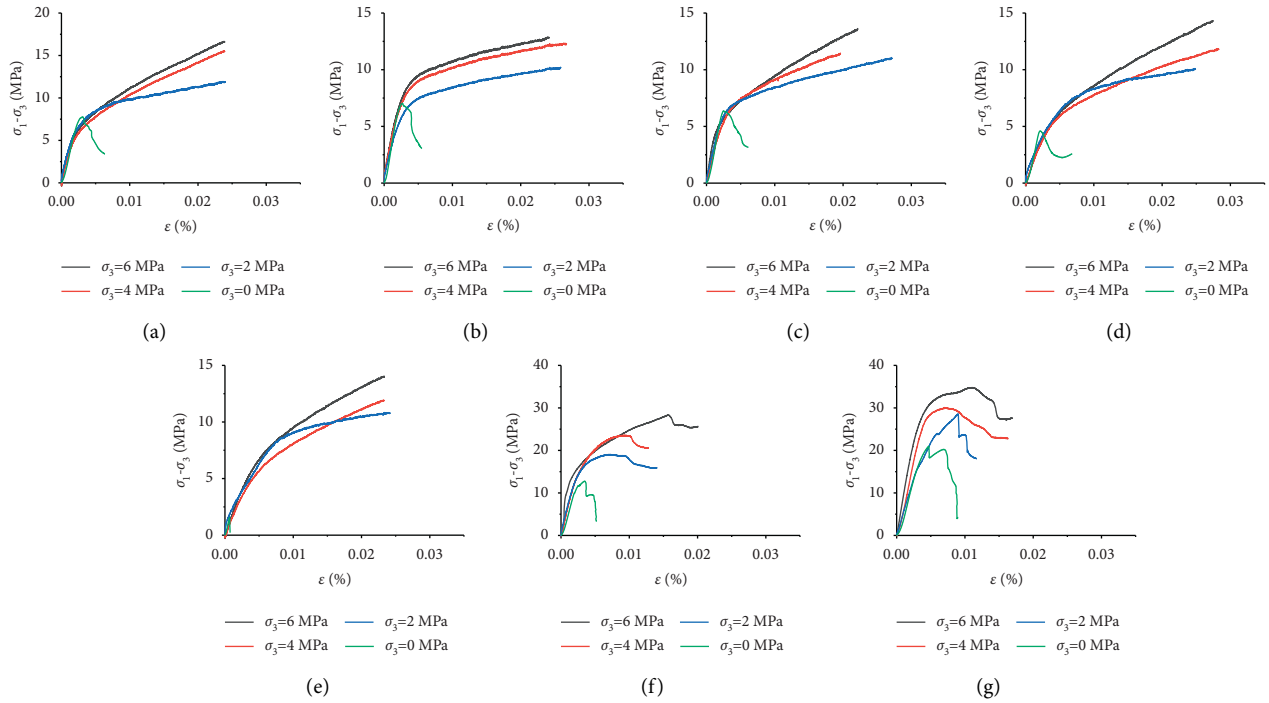


FIGURE 8: Stress-strain curves of Group AC layered composite rock under triaxial compression: (a) $\beta = 0^\circ$, (b) $\beta = 15^\circ$, (c) $\beta = 30^\circ$, (d) $\beta = 45^\circ$, (e) $\beta = 60^\circ$, (f) $\beta = 75^\circ$, and (g) $\beta = 90^\circ$.

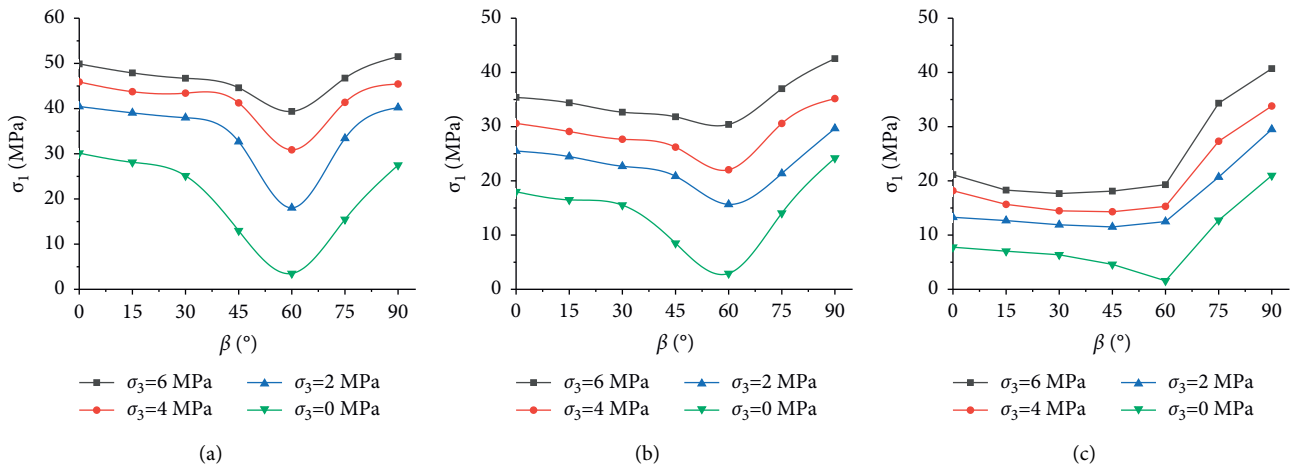


FIGURE 9: Effect of the bedding plane inclination on peak strength: (a) Group AA, (b) Group AB, and (c) Group AC.

conditions. The $\beta = 90^\circ$ specimens exhibited axial splitting failure (Type I) at lower confining pressures ($\sigma_3 = 0-2$ MPa), whereas at high confining pressures ($\sigma_3 = 4, 6$ MPa), the rupture mode was diagonal shear failure in the bedding plane direction (Type III).

Figure 11(b) shows the failure mode of the composite rock mass of Group AB under different confining pressures. The specimens with lower bedding dip angles ($\beta = 0^\circ-30^\circ$) showed Y-shaped splitting failure (Type V) under different confining pressures. The strengths of the two rock layers A and B in the specimens were different, resulting in cracks mainly in the lower strength layer B. The specimens with

$\beta = 5^\circ$ exhibited slip failure in the stratification direction (Type II) under no confining pressure ($\sigma_3 = 0$ MPa). When confining pressure was applied ($\sigma_3 = 2-6$ MPa), the specimens exhibited coupled slip and axial splitting along the bedding plane (Type IV), and cracks only appeared in the weaker B formations. The specimens with $\beta = 60^\circ$ to 75° exhibited slip damage along the bedding plane under different confining pressures. The $\beta = 90^\circ$ specimens all showed axial splitting failure (Type I) at lower confining pressures ($\sigma_3 = 0-2$ MPa), whereas at confining pressures of $\sigma_3 = 4-6$ MPa, the primary fracture mode was diagonal shear failure in the bedding plane (Type III).

TABLE 2: Anisotropic classification [18].

The range of anisotropy ratio R_c	Anisotropic grade of rock
$1.0 \leq R_c \leq 1.1$	Isotropy
$1.1 \leq R_c \leq 2.0$	Low anisotropy
$2.0 \leq R_c \leq 4.0$	Medium anisotropy
$4.0 \leq R_c \leq 6.0$	High anisotropy
$6.0 \leq R_c$	Very high anisotropy

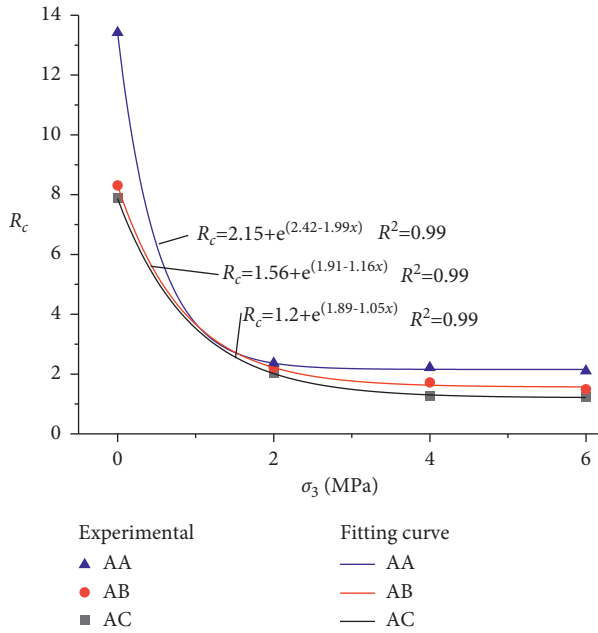


FIGURE 10: Relationship between the anisotropy ratio and the confining pressure.

Figure 11(c) shows the failure mode of the composite rock masses of the AC group under different confining pressures. The specimens with a lower bedding angle ($\beta = 0^\circ - 30^\circ$) showed Y-shaped splitting failure (Type V) under no confining pressure. After the confining pressure was applied ($\sigma_3 = 2-6$ MPa), unlike the first two groups, the damage to the specimens only occurred in the C formation, whereas no damage was observed in the A formation, indicating shear damage in the weak layer (Type VI). The reason is that the strength of the C formation is much less than that of the A formation; thus, the former is more likely to be damaged in the weak layer under confining pressure. The $\beta = 45^\circ - 75^\circ$ specimens under different confining pressures exhibited slip failure in the stratification direction (Type II). The $\beta = 90^\circ$ specimens showed axial splitting failure (Type I) under uniaxial loading, whereas under confining pressure ($\sigma_3 = 2-6$ MPa), the dominant rupture mode was diagonal shear failure in the bedding plane (Type III).

The experimental results show that the bedding angle and lithological composition are the dominant factors influencing the compressional fracture behavior of the layered rock masses under triaxial compression.

5. Discussion of the Strength Characteristics

The linear Mohr–Coulomb strength criterion [19] is the most widely used strength criterion in rock mechanics. It is defined as

$$\tau = c + \sigma \tan \varphi, \quad (2)$$

where τ is the shear strength of the rock, σ is the positive stress in the shear plane, and c and φ are the cohesion and angle of the internal friction of the rock material, respectively.

The Mohr–Coulomb criterion can be rewritten in the form of principal stresses as

$$\sigma_1 = \sigma_3 \tan^2\left(45^\circ + \frac{\varphi}{2}\right) + 3c \tan\left(45^\circ + \frac{\varphi}{2}\right). \quad (3)$$

Equation (3) can be used to describe the strength of different groups of specimens under triaxial stress conditions as follows:

$$\sigma_{1(\beta)} = k_{(\beta)} \sigma_3 + \sigma_{c(\beta)}, \quad (4)$$

where σ_1 and σ_3 are the maximum and minimum principal stresses at the failure of the rock mass, respectively, σ_c is the uniaxial compressive strength of the rock specimen, and k is a coefficient.

The characteristic strength values of the three groups of layered specimens in Figure 8 at different confining pressures were fitted using the Mohr–Coulomb strength criterion. The results are shown in Figure 12. The calculated coefficients of the Mohr–Coulomb criterion for each group of rocks are listed in Table 3. The correlation coefficients ranged from 0.85 to 0.98.

Although the Mohr–Coulomb criterion is straightforward and has a clear physical meaning, it has limited application because it is based on the assumption that the cohesion and internal friction angle of the rock are constant during the test. Due to the anisotropic nature of the composite formation specimens and the nonlinear behavior of the confining pressure and peak strength, the Hoek–Brown strength criterion [20] is used in a nonlinear regression of the triaxial peak strengths for the three sets of specimens. This criterion was first proposed by Hoek and Brown in 1980 as an empirical strength criterion for intact rocks based on the results of triaxial tests on hundreds of sets of rocks. A generalized Hoek–Brown strength criterion was later proposed based on a large number of field rock tests [21]. It is defined in

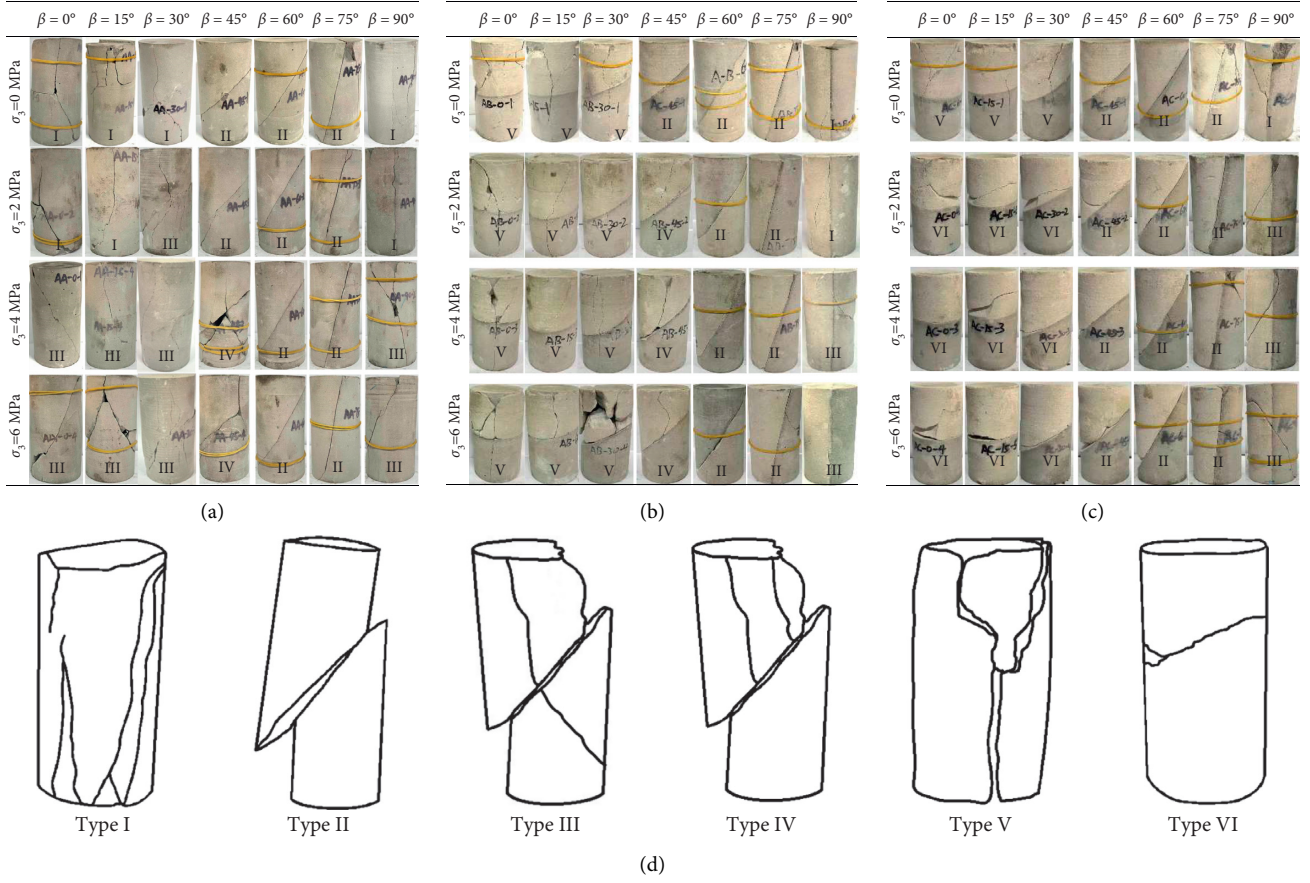


FIGURE 11: Failure modes of the composite layered samples under different confining pressures. (a) Group AA, (b) Group AB, (c) Group AC, and (d) failure mode classification (please enlarge the view when observing).

$$\sigma_1 = \sigma_3 + \sigma_{ci} \left(\frac{m_b \sigma_3}{\sigma_{ci}} + s \right)^\alpha, \quad (5)$$

where σ_1 and σ_3 are the maximum and minimum principal stresses in a rock sample at failure, σ_{ci} is the uniaxial compressive strengths of the rock sample, and m_b , m_b , s , and α are constants related to the properties of the rock mass. Equation (5) can also be expressed as

$$(\sigma_1' - \sigma_3')^2 = m_i \sigma_{ci} \sigma_3' + \sigma_{ci}^2. \quad (6)$$

By setting $x = \sigma_3'$ and $y = (\sigma_1' - \sigma_3')^2$, we obtain

$$y = m \sigma_{ci} x + s \sigma_{ci}^2, \quad (7)$$

$$\sigma_{ci}^2 = \frac{\sum y}{n} - \left\{ \frac{\sum xy - (\sum x \sum y/n)}{\sum x^2 - [(\sum x)^2/n]} \right\} \frac{\sum x}{n},$$

$$m_i = \frac{1}{\sigma_{ci}} \frac{\sum xy - (\sum x \sum y/n)}{\sum x^2 - [(\sum x)^2/n]}.$$

The squared correlation coefficient is

$$R^2 = \frac{[\sum xy - (\sum x \sum y/n)]^2}{[\sum x^2 - ((\sum x)^2/n)][\sum y^2 - ((\sum y)^2/n)]}. \quad (8)$$

When the rock sample is an intact rock, we set $m_b = m_i$, $\alpha = 0.5$, and $s = 1$. The expression is

$$\sigma_1 = \sigma_3 + \sigma_{ci} \left(\frac{m_i \sigma_3}{\sigma_{ci}} + 1 \right)^{0.5}. \quad (9)$$

Based on this equation, the strength of the specimens with different inclination angles can be described as

$$\sigma_{1(\beta)} = \sigma_{3(\beta)} + \sigma_{c(\beta)} \left(\frac{m_{i(\beta)} \sigma_{3(\beta)}}{\sigma_{c(\beta)}} + 1 \right)^{0.5}, \quad (10)$$

where $\sigma_{c(\beta)}$, $\sigma_{1(\beta)}$, $\sigma_{3(\beta)}$, and $m_{i(\beta)}$ are the uniaxial compressive strength, maximum principal stress, minimum principal stress, and parameters from the Hoek-Brown criterion for specimens with different inclination angles, respectively. The corresponding $m_{i(\beta)}$ and $\sigma_{c(\beta)}$ of the criterion can be derived for each angle of the specimens. The calculated values are listed in Table 4, and the fitting results are shown in Figure 13. R^2 ranges from 0.96 to 0.99,

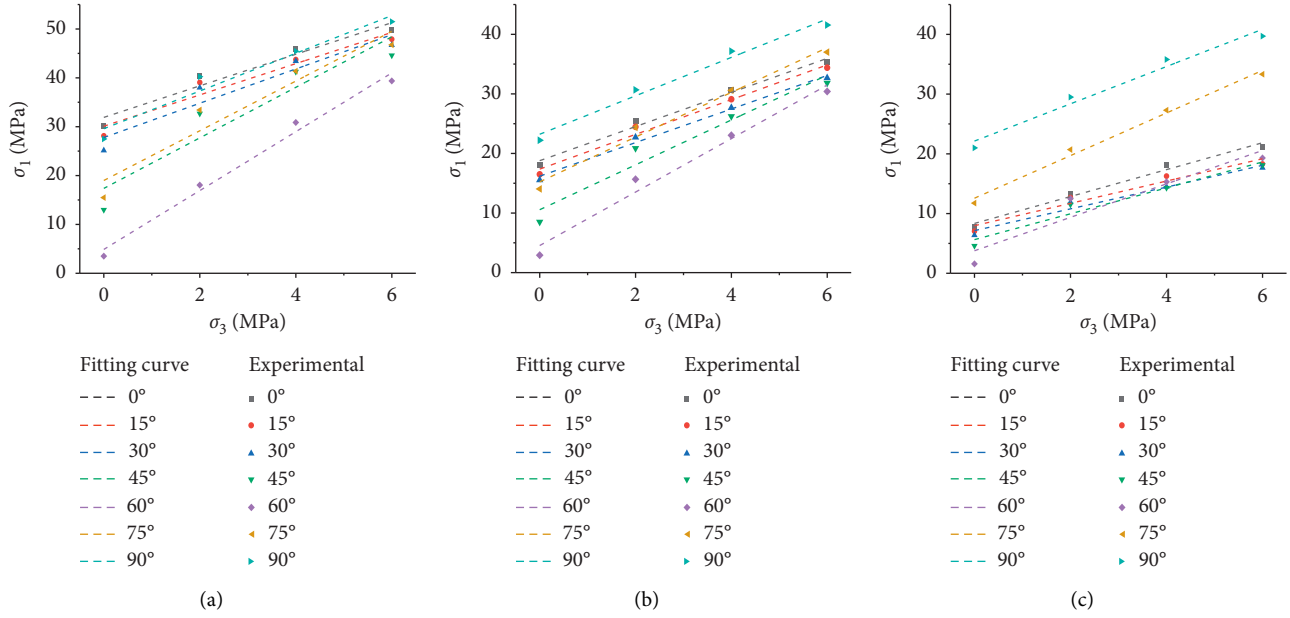


FIGURE 12: Fitting curve of the linear Mohr–Coulomb strength criterion. (a) Group AA, (b) Group AB, and (c) Group AC.

TABLE 3: The calculated coefficients of the Mohr–Coulomb criteria for different groups of rocks.

	β	0°	15°	30°	45°	60°	75°	90°
AA	k	3.23	3.2	3.5	5.17	6.02	5.08	3.86
	R^2	0.95	0.94	0.9	0.88	0.98	0.92	0.95
AB	k	2.86	2.91	2.81	3.7	4.49	3.75	3.22
	R^2	0.98	0.97	0.98	0.92	0.96	0.97	0.97
AC	k	2.25	1.86	1.82	2.16	2.80	3.56	3.12
	R^2	0.97	0.93	0.95	0.94	0.85	0.98	0.96

TABLE 4: The calculated coefficients of the Hoek–Brown empirical criterion.

	β	0°	15°	30°	45°	60°	75°	90°
AA	m_i	7.35	6.59	8.23	20.79	48.91	17.58	8.74
	$\sigma_{c(\beta)}$	30.13	28.12	25.21	12.98	3.49	15.47	27.49
	R^2	0.96	0.96	0.96	0.97	0.99	0.98	0.97
AB	m_i	5.25	5.58	5.22	12.6	31.92	9.29	6.29
	$\sigma_{c(\beta)}$	18.01	16.50	15.48	8.49	2.92	14.04	24.20
	R^2	0.99	0.99	0.99	0.98	0.99	0.99	0.99
AC	m_i	4.0	3.1	2.79	4.95	21.41	7.56	6.14
	$\sigma_{c(\beta)}$	7.77	7.04	6.37	4.60	1.56	12.74	20.99
	R^2	0.99	0.98	0.98	0.98	0.97	0.99	0.98

indicating higher accuracy than that obtained from the Mohr–Coulomb strength criterion (0.85 to 0.98). A comparison of the R^2 values of the fitting results based on the two criteria is shown in Figure 14. The results indicate that the Hoek–Brown strength criterion has higher accuracy for predicting the failure strength characteristics of the composite rock specimens under different confining pressures.

Both sides of (10) are divided by $\sigma_{c(\beta)}$ to obtain a dimensionless parameter independent of the uniaxial compressive strength:

$$\frac{\sigma_{1(\beta)}}{\sigma_{c(\beta)}} = \frac{\sigma_{3(\beta)}}{\sigma_{c(\beta)}} + \left(\frac{m_{i(\beta)} \sigma_{3(\beta)}}{\sigma_{c(\beta)}} + 1 \right)^{0.5}. \quad (11)$$

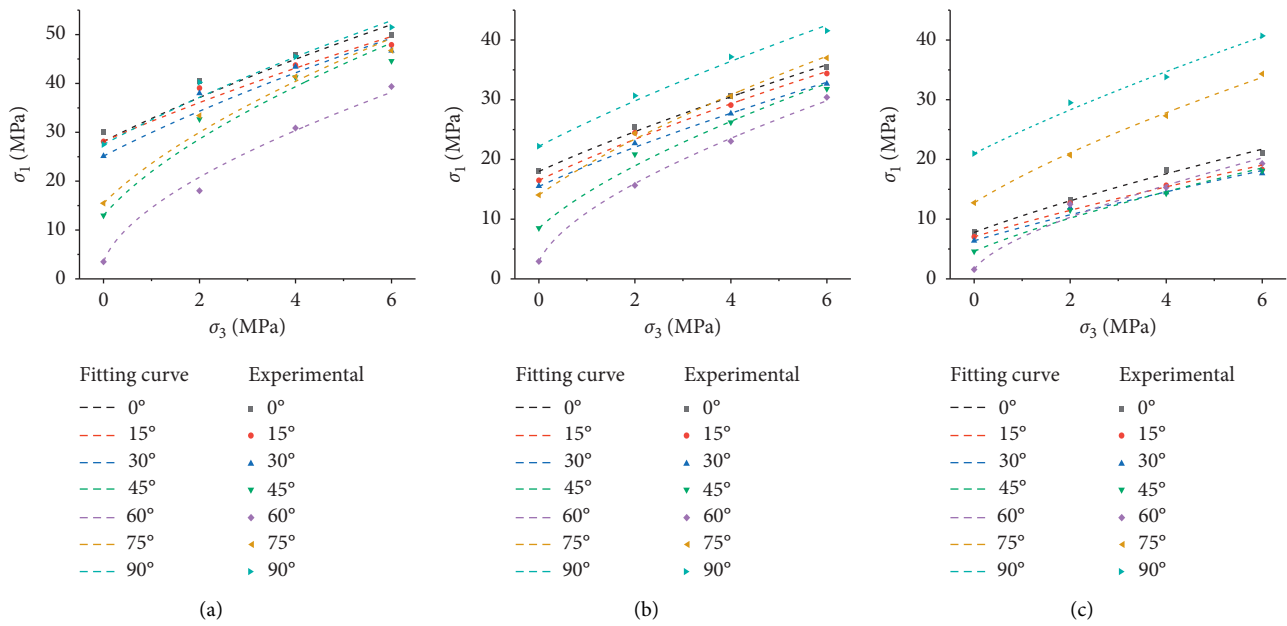


FIGURE 13: Fitting curve of the Hoek–Brown strength criterion. (a) Group AA, (b) Group AB, and (c) Group AC.

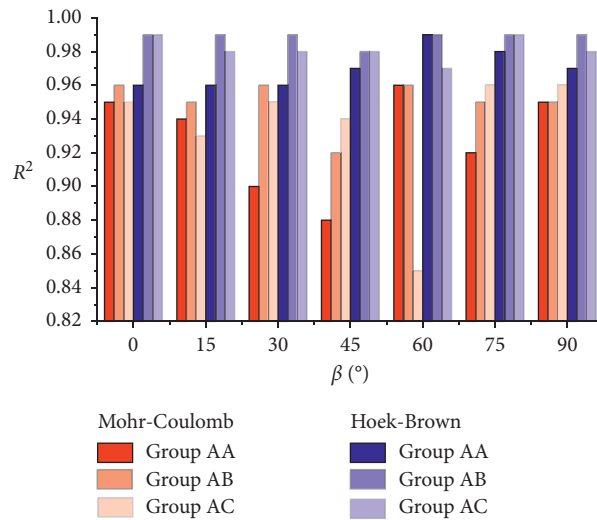


FIGURE 14: Error analysis of the fitting results using the two strength criteria.

The Hoek–Brown strength curve is standardized by substituting the parameters $m_{i(\beta)}$ of the specimen with different inclination angles (Table 2) into (11), as shown in Figure 15.

With the increasing of confining pressure, the closer the curve is, the lower the strength anisotropy of the specimen is, and conversely, the far the curve is, the more pronounced the

anisotropy is. The specimens with $\beta = 60^\circ$ in all three groups show the most significant increase in the strength difference with an increase in the confining pressure. It can be inferred that the nonlinear variation of the peak strength with the confining pressure becomes more pronounced as the confining pressure increases.

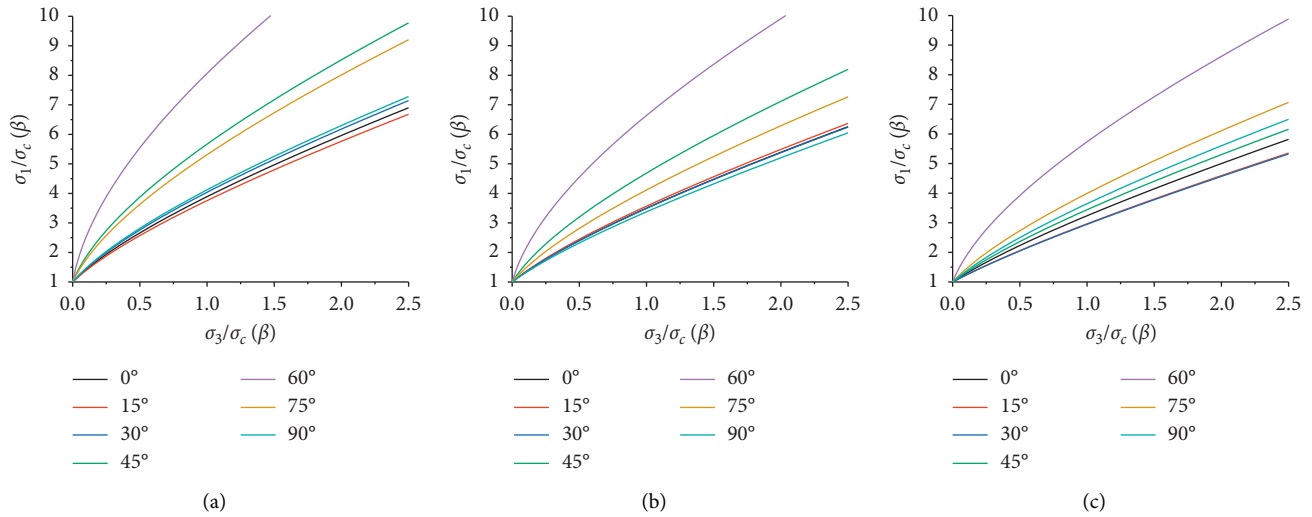


FIGURE 15: Dimensionless standardized Hoek–Brown strength curve. (a) Group AA, (b) Group AB, and (c) Group AC.

6. Conclusion

We used 3D scanning and 3DP to prepare composite specimens with a bedding structure and three different strengths and conducted triaxial compression tests to investigate the strength anisotropy and deformation of the composite rocks. We analyzed the failure mode and failure mechanism of the composite specimens. The conclusions are as follows.

- (1) The bedding angle and composition substantially influenced the failure mode of the rock body. When the lithology of the two layers was similar, the rock body exhibited axial splitting (Type I), diagonal shear failure in the bedding plane (Type III), and slip failure in the stratification direction (Type II) for bedding angles of $[0^\circ\text{--}90^\circ]$. When the lithology of the two layers was dissimilar, slip failure and axial splitting occurred along the bedding plane (Type IV), and Y-shaped splitting (Type V) and shearing in the weak layers (Type VI) were observed due to the weaker rock mass. The failure mode and mechanical properties depended on the rock mass, the rock formation, and the stress state.
- (2) The stress-strain curves and peak strengths of the composite specimens with layered structures showed anisotropic characteristics corresponding to their failure modes. As the bedding angle increased, the peak strength of the three groups of specimens showed an asymmetric “U”-shaped curve that first decreased and then increased under different confining pressure levels. The peak strength of the specimens was linearly related to the confining pressure, and the difference in the compressive strength of the specimens with different bedding angles decreased as the confining pressure level increased.
- (3) The anisotropy of the rock strength gradually decreased with increasing confining pressure,

evidenced by (a) a decrease in the anisotropy coefficient R_c with increasing confining pressure and (b) a change in failure mode from slips along the joints to block damage with increasing confining pressure, as in the case of the specimens with a bedding angle of $\beta = 45^\circ$.

- (4) The Hoek–Brown strength criterion provided better performance than the Mohr–Coulomb strength criterion for predicting the nonlinear failure strength characteristics of the composite specimens at different confining pressures. The specimens with $\beta = 60^\circ$ in all three groups showed the most significant increase in strength with increasing confining pressure.

Data Availability

The data used to support the findings of this study are available from the corresponding author upon request.

Conflicts of Interest

The authors declare that they have no conflicts of interest.

Acknowledgments

The work described in this paper was fully supported by National Natural Science Foundation of China (51674100).

References

- [1] J. Zhang, “Borehole stability analysis accounting for anisotropies in drilling to weak bedding planes,” *International Journal of Rock Mechanics and Mining Sciences*, vol. 60, pp. 160–170, 2013.
- [2] G. Barla, “Full-face excavation of large tunnels in difficult conditions,” *Journal of rock mechanics and geotechnical engineering*, vol. 8, no. 3, pp. 294–303, 2016.
- [3] S. R. Wang, X. G. Wu, Y. H. Zhao, and P. Hagan, “Evolution characteristics of composite pressure-arch in thin bedrock of

- overlying strata during shallow coal mining,” *International Journal of Applied Mechanics*, vol. 11, no. 3, Article ID 1950030, 2019.
- [4] Y. M. Tien, M. C. Kuo, and C. H. Juang, “An experimental investigation of the failure mechanism of simulated transversely isotropic rocks,” *International Journal of Rock Mechanics and Mining Sciences*, vol. 43, no. 8, pp. 1163–1181, 2006.
- [5] A. Tavallali and A. Vervoort, “Effect of layer orientation on the failure of layered sandstone under Brazilian test conditions,” *International Journal of Rock Mechanics and Mining Sciences*, vol. 47, no. 2, pp. 313–322, 2010.
- [6] B. Debecker and A. Vervoort, “Experimental observation of fracture patterns in layered slate,” *International Journal of Fracture*, vol. 159, no. 1, pp. 51–62, 2009.
- [7] E. Hoek, *Underground Excavations in Rock*, The Institute of Mining and Metallurgy, Kuala Lumpur, Malaysia, 1980.
- [8] R. Mclamore and K. E. Gray, “The mechanical behavior of anisotropic sedimentary rocks,” *Journal of Engineering for Industry*, vol. 89, no. 1, pp. 62–73, 1967.
- [9] T. Ramamurthy, “Strength and modulus responses of anisotropic rocks,” *Comprehensive rock engineering*, vol. 1, no. 13, pp. 313–329, 1993.
- [10] R. Nova, “The failure of transversely isotropic rocks in triaxial compression,” *International Journal of Rock Mechanics and Mining Science & Geomechanics Abstracts*, vol. 17, no. 6, pp. 325–332, 1980.
- [11] Y. M. Tien and P. F. Tsao, “Preparation and mechanical properties of artificial transversely isotropic rock,” *International Journal of Rock Mechanics and Mining Sciences*, vol. 37, no. 6, pp. 1001–1012, 2000.
- [12] X. Chang and Y. Deng, “Experimental study of reinforced layered rocks with a hard-weak-hard structure under compression,” *International Journal of Geomechanics*, vol. 20, no. 11, Article ID 4020203, 2020.
- [13] S. Fereshtenejad and J. J. Song, “Applicability of powder-based 3D printing technology in shear behavior analysis of rock mass containing non-persistent joints,” *Journal of Structural Geology*, vol. 143, Article ID 104251, 2020.
- [14] J. B. Zhu, T. Zhou, Z. Y. Liao, L. Sun, X. B. Li, and R. Chen, “Replication of internal defects and investigation of mechanical and fracture behaviour of rock using 3D printing and 3D numerical methods in combination with X-ray computerized tomography,” *International Journal of Rock Mechanics and Mining Sciences*, vol. 106, pp. 198–212, 2018.
- [15] Y. Ju, L. Wang, H. Xie, G. Ma, Z. Zheng, and L. Mao, “Visualization and transparentization of the structure and stress field of aggregated geomaterials through 3D printing and photoelastic techniques,” *Rock Mechanics and Rock Engineering*, vol. 50, no. 6, pp. 1383–1407, 2017.
- [16] Q. Jiang, X. Feng, Y. Gong, L. Song, S. Ran, and J. Cui, “Reverse modelling of natural rock joints using 3D scanning and 3D printing,” *Computers and Geotechnics*, vol. 73, pp. 210–220, 2016.
- [17] National Standards of the People’s Republic of China, *Standard For Engineering Classification of Rock masses (GB/T50218-2014)*, Ministry of Housing and Urban-Rural Development of the People’s Republic of China, Beijing, China, 2014.
- [18] J. Singh, T. Ramamurthy, and R. V. Rao, “Strength anisotropies in rocks,” *Indian Geotechnical Journal*, vol. 19, no. 2, pp. 147–166, 1989.
- [19] P. Barsanescu, A. Sandovici, and A. Serban, “Mohr-Coulomb criterion with circular failure envelope, extended to materials with strength-differential effect,” *Materials & Design*, vol. 148, pp. 49–70, 2018.
- [20] E. Hoek and E. T. Brown, “Empirical strength criterion for rock masses,” *Journal of the Geotechnical Engineering Division*, vol. 106, no. 9, pp. 1013–1035, 1980.
- [21] E. Hoek, C. T. Carranza-Torres, and B. Corkum, “Hoek-Brown failure criterion-2002 edition,” in *Proceedings of the fifth North American rock mechanics symposium*, vol. 1, pp. 267–273, Toronto, Canada, January, 2002.